

UAV ICING: ICE ACCRETION EXPERIMENTS AND VALIDATION

Richard Hann¹

¹Norwegian University of Science and Technology (NTNU)

Abstract

Atmospheric icing is a key challenge to the operational envelope of medium-sized fixed-wing UAVs. Today, several numeric icing codes exist, that all have been developed for general aviation applications. UAVs with wingspans of several meters typically operate at Reynolds numbers an order of magnitude lower than commercial and military aircraft. Therefore, the question arises to what extent the existing codes can be applied for low-Reynolds UAV applications to predict ice accretion. This paper describes an experimental campaign at the Cranfield icing wind tunnel on a RG-15 and a NREL S826 airfoil at low velocities (25–40m/s). Three meteorological icing conditions have been selected to represent the main ice typologies: rime, glaze, and mixed ice. Each case has been run at least twice in order to assess the repeatability of the experiments. Manual ice shape tracings have been taken at three spanwise locations for each icing case. The liquid water content calibration was performed according to ARP5905 using the icing blade method. The tests have initially shown significantly higher water contents than anticipated, which could be traced to dimensional differences of the blade at Cranfield, as well as low flow velocities. This systematic error was resolved by simulating the droplet collection coefficients on the off-specification blade. In addition to manual tracings, photogrammetry and a handheld laser-scanner were used to capture the ice shapes. The results indicate that manual tracings are still the most efficient method, although there is potential in exploring the alternatives further. Additionally, numerical simulations with two icing codes, LEWICE and FENSAP-ICE, were performed on a rime and a glaze case. For rime, the simulations show a good agreement with the experiment, whereas the glaze case exhibits significant differences.

Introduction

Atmospheric in-cloud icing is a severe hazard for all types of aircraft. In particular, medium-sized fixed-wing unmanned aerial vehicles (UAVs) with wings spans of few meters are limited in their operational envelope by icing [1]. These types of UAVs are usually designed for long-range and long-endurance missions that often require all-weather capabilities. Example applications for such UAVs are remote sensing in cold climates, ship-based iceberg detection, oil spill response, or search & rescue [2]. Today, there is no mature icing protection system available for this category of UAVs. Effectively, UAVs have to stay grounded when icing conditions are expected during a mission, or else they are exposed to severe hazards and the risk of losing the vehicle [3].

Icing in general aviation is a well-studied process [4], whereas little research has been conducted for UAVs. One of the main differences is that most UAVs, except for the largest, operate at significantly lower flight velocities and altitudes compared to the general aviation,

Page 1 of 8

and are smaller in size. The Reynolds numbers occurring during UAV icing are therefore an order of magnitude lower compared to icing on commercial or military aircraft. This difference in the flow physics is likely to play an important role for the icing process [5], which justifies the need for dedicated research.

At this point, very limited work has been performed on UAV icing. Most existing studies are using different numerical methods to investigate icing on fixed-wing UAVs (e.g. [6–9]). Numerical icing simulation tools are a good approach for studying the effects of icing on aerodynamic performance. Numerical models also play an important role for the design of efficient icing protection systems [10]. Several icing simulation tools have been developed for the use in general aviation but have so far not been validated for the application on UAVs. This is partly due to the lack of experimental data, as very sparse information on UAV icing exists in the open literature. Up to now, only a single study on the ice accretion on a UAV airfoil [11] is available, whereas a few more exist for icing on UAV propellers [12].

This paper describes a test campaign that has been conducted in the icing wind tunnel at Cranfield University with the aim to generate ice shape validation data for icing on fixed-wing UAV airfoils. A key characteristic of such data is the requirement of a high level of accuracy and confidence. Since previous work has found that ice shapes may show high degrees of variability [13], another objective was to investigate the consistency of the experimental ice shapes with regards to spanwise distribution and repeatability of tests. In addition, different methods to measure the ice shapes were tested with the aim to obtain higher fidelity ice shapes for the validation process.

It should be noted that icing at low Reynolds numbers is also occurring on small to mid-sized wind turbines [14]. There are several similarities between wind turbine icing and UAV icing, especially the lack of experimental data for validation. For this reason, tests were also conducted on a wind turbine airfoil. This also yields insights into how different airfoil parameters may influence ice accretion.

Method

Ice accretion tests have been performed in the Cranfield icing wind tunnel [15] on rectangular airfoil models, as shown in Fig. 1. The facilities at Cranfield offer a test section of $0.76 \times 0.76\text{m}$ and the

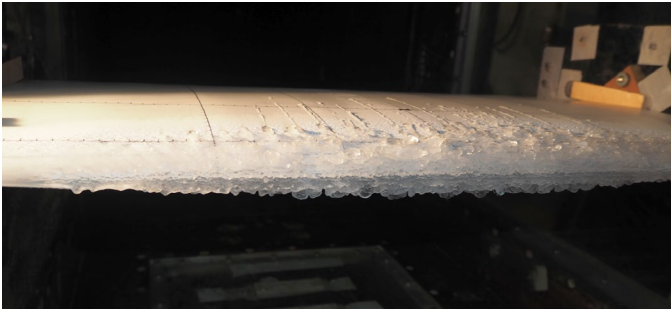


Figure 1. RG-15 airfoil model mounted in the wind tunnel with mixed ice accretions and some runback ice visible.

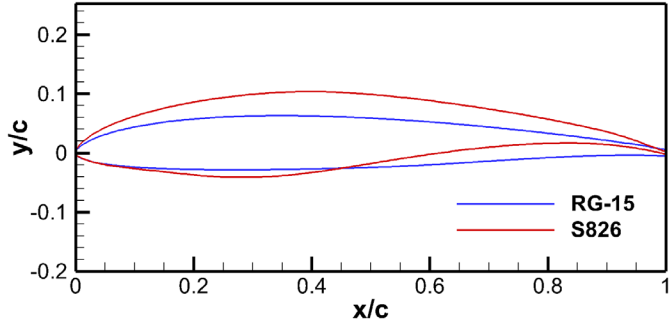


Figure 2. Comparison of the RG-15 and S826 airfoil geometries.

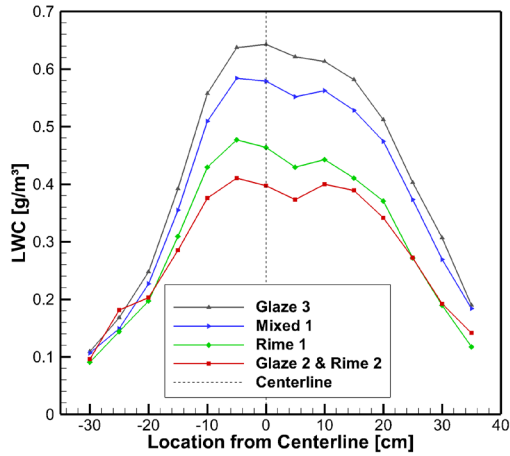


Figure 3. Spanwise liquid water content distribution in the wind tunnel test section for the test cases at $v=25\text{m/s}$ and $MVD=20\mu\text{m}$.

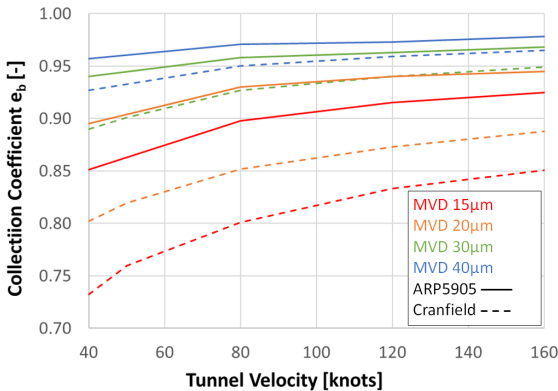


Figure 4. Comparison of the collision coefficient of the original ARP5905 blade to the Cranfield blade for different MVDs and flow velocities.

capability to provide total temperatures from $T=-30\ldots+30^\circ\text{C}$, liquid water concentrations from $LWC=0.05\ldots3\text{g/m}^3$ and droplet sizes from $MVD=15\ldots80\mu\text{m}$. The tunnel can generate wind speeds in the Mach number range of $Ma=0.1\ldots0.5$, enabling the tunnel to be used for aerospace, automotive, and wind energy application. A particle size distribution record was provided for the nominal droplet diameter setting of $20\mu\text{m}$, stating $DV(10)=7.93\mu\text{m}$, $DV(50)=19.06\mu\text{m}$, $DV(90)=32.70\mu\text{m}$, and a relative span of $RS=1.30$.

Two airfoil models have been investigated, both with a chord length of $c=0.45\text{m}$: an NREL S826 wind turbine airfoil with a span of $b=0.50\text{m}$, and an RG-15 UAV airfoil with a span of $b=0.76\text{m}$. Figure 2 shows the two airfoil geometries. A total of 25 ice accretion runs have been performed with 9 runs on the S826 and 16 on the RG-15. A general guideline in choosing the icing test conditions has been to generate ice shapes representing the three main ice morphologies: rime, glaze, and mixed ice. In order to build confidence in the data, the repeatability of the experiments has been tested by running identical conditions multiple times. An overview of the icing conditions that have been tested is given in Table 1.

For each test, three manual ice shape tracings have been taken in order to assess the spanwise variability. One measurement has been taken at the centerline of the test section, one at -10cm to the left (looking downstream) of it, and $+10\text{cm}$ to its right. In addition, for each tracing, the maximum thickness of the ice has been measured with a caliper on the leading-edge. Post-processing of the manual tracings includes the digitalization of the ice contours using the software WebPlotDigitizer [16]. The resulting data were further processed with Matlab to calculate the total ice area, the ice thickness, and the icing limits. The latter two values are given in relation to the distance s from the upper trailing-edge.

Supporting numerical icing simulations have been conducted with LEWICE (version 3.2.2) and FENSAP-ICE (version 19.2). LEWICE is a 1st generation icing code developed by NASA based on a panel method for general aviation applications. The code is technically not validated for low Reynolds numbers ($Re_{min}=2.26 \cdot 10^6$) but has been applied for UAV applications before [6,10]. ANSYS FENSAP-ICE is a 2nd generation icing simulation code based on modern CFD methods [17]. The code is suitable for a wide range of applications, but with limited reported validation data. The FENSAP-ICE simulations have been performed with hybrid 2D meshes, consisting of a structured boundary layer and an unstructured far field. The Spalart-Allmaras turbulence model was used for all cases. In the scope of this work, all simulations were conducted with monodisperse droplet distributions and multi-shot icing simulations.

LWC Calibration

The calibration of the LWC in the tunnel was performed according to the icing blade method described in ARP5905 [18]. With this method, a blade was inserted into the icing tunnel at very low temperatures ($T>-18^\circ\text{C}$) for a short period of time (1–2min). The LWC in the airstream can be estimated by measuring the thickness of the accumulated ice along the blade and the following equation:

$$LWC_{blade} = \frac{\rho_{ice} \tau_{ice}}{e_{blade} v t}$$

Table 1. Overview of different icing condition configurations and liquid water contents before and after the correction.

Case	v [m/s]	T [°C]	MVD [μm]	Target LWC [g/m³]	Initial LWC [g/m³]	Corrected LWC [g/m³]	e_{blade} [-]
Glaze 1	25	-2	30	0.34	0.38	0.46	0.90
Glaze 2	25	-2	20	0.34	0.38	0.51	0.82
Glaze 3	25	-2	20	0.59	0.60	0.80	0.82
Rime 1	25	-10	20	0.43	0.42	0.56	0.82
Rime 2	25	-15	20	0.32	0.38	0.51	0.82
Mixed 1	25	-5	20	0.53	0.54	0.72	0.82
Mixed 2	40	-4	20	0.55	0.58	0.75	0.85
Mixed 3	40	-5	20	0.2	0.33	0.43	0.85

with the density of ice ρ_{ice} , the ice thickness accumulated on the blade τ_{ice} , the blade collection coefficient e_{blade} , the test section velocity v , and the blade exposure time t . During the initial calibrations, the collection coefficient was assumed as $e_{blade}=1$ and ice density as $\rho_{ice}=800\text{kg/m}^3$. For flow velocities of $v=25\text{m/s}$, the exposure time was selected as $t=120\text{s}$. For the higher velocities of $v=40\text{m/s}$ the time was reduced to $t=60\text{s}$. An example of the resulting initial LWC distribution on the blade is shown in Fig. 3 for the nozzle configuration of $v=25\text{m/s}$ and $MVD=20\mu\text{m}$. The distribution shows a significant variability across the wind tunnel test section. Relatively constant values are reached near the centerline location where the ice shapes were measured.

After the first few icing runs substantially larger ice accretions were observed, compared to what was expected from previous simulation results. The resulting ice thicknesses were more than double as high as anticipated based on prior LEWICE and FENSAP-ICE simulations. While differences between simulation and experiment were expected, the magnitude of these differences exceeded what could be accounted for model errors. This has led to the investigation of the LWC calibration procedure.

A key discovery was that the blade used for calibration at Cranfield had different dimensions ($6.3\times15.8\text{mm}$) compared to the blade specified in ARP5905 ($3.2\times50.8\text{mm}$). A different blade geometry, especially the almost doubled thickness, is likely to affect the blade collection coefficient. In order to investigate this effect, we followed the same procedure as in ARP5905 to determine the collection coefficients. LEWICE calculations on the Cranfield and the ARP5905 blade geometry were conducted for different values of MVD and flow velocities. Figure 4 compares the results for both blade shapes. The simulations show that the thicker blade is leading to a significantly reduced droplet collection efficiency. This effect is largest for small droplets with reduced inertia, that are more easily deflected by the flow field around the airfoil. For the $MVD=20\mu\text{m}$ and $v=25\text{m/s}$ case the simulation results yield blade collection coefficients of $e_{blade,Cranfield}=0.82$ compared to $e_{blade,ARP5905}=0.91$. This shows that the actual blade collection coefficient of the Cranfield blade can result in a more than 20% LWC increase compared to the initial ($e_{blade}=1$) calibration. Confidence in the simulation data is added by the good match of the ARP5905 results with the literature values [18]. In addition, FENSAP-ICE simulations have been run for selected cases, and fully supported the LEWICE results.

Another discussion point in the calibration was the choice of ice density. The recommended value from ARP5905 is $\rho_{ice}=880\text{kg/m}^3$ which is 10% higher than the value used in the initial calibration. The literature suggests that ice densities can vary significantly [19,20],

especially for rime ice. A more recent study by Vargas et al. [21] using a x-ray contact micro-radiography method to determine ice densities of rime, glaze, and mixed suggest that a density of $\rho_{ice}=880\text{kg/m}^3$ can be assumed for all ice types. Without explicit data from the Cranfield tunnel on ice densities on the calibration blade, we believe that it is justified to use the higher density for the LWC calibration.

Table 1 shows an overview of all the tunnel configurations used in this study. The target LWC is the nominal value that has been specified before the tests, the initial LWC is what has been achieved after the initial calibration, and the corrected LWC includes adjustments of blade collection coefficient and ice density. Depending on airspeed and droplet size, the real achieved LWC values are between 31–114% higher than the originally targeted LWC.

Icing Simulation

Numerical icing simulations have been conducted and compared to the experimental ice shapes. This preliminary validation has been performed on a run with a “Rime 2” and a “Glaze 1” configuration. The first case (run #11) was chosen because it was conducted at very low temperatures ($T=-15^\circ\text{C}$), which ensures instantaneous freezing of all droplets upon impact on the airfoil surface. This type of icing has been shown to be the easiest to simulate numerically due to its simple icing mechanism [22]. Simulations have been carried out with LEWICE and FENSAP-ICE for different LWC values: the initial value prior to correction ($LWC=0.31\text{g/m}^3$) and the corrected value considering the blade collection coefficient and adjusted ice density ($LWC=0.51\text{g/m}^3$). Further, an LWC value was determined based on the simulation results that would match the experimental ice shape thickness best. The outcome for LEWICE is shown in Fig. 5 and for FENSAP-ICE in Fig. 6.

The results show clearly how large the difference between the expected ice shapes and the actual ice was. Using the initial LWC, LEWICE predicts a maximum ice thickness of 8.4mm and FENSAP-ICE 7.6mm, whereas the experimental measurements indicate ice thicknesses between 12–14mm. With the adjusted LWC values, LEWICE predicts a thickness of about 11.1mm whereas FENSAP-ICE matches the experiments well with 13.2mm. To match the experiments with LEWICE, the LWC had to be increased till 0.61g/m^3 . Both codes are significantly underpredicting the total ice area and the icing limits on the upper surface. The experimental ice shapes also exhibit a more irregular and more rugged surface compared to the smooth numerical simulation results.

Figure 7 shows the simulation outcomes for a glaze case (run #14) with the corrected LWC value. Neither of the codes is seemingly able to predict the experimental ice shapes with high accuracy. The LEWICE result exhibits a significantly smoother surface with a comparatively lower ice area. FENSAP-ICE generates a T-shaped horn which is not detectable (as distinct) in the experimental data. While the surface in FENSAP-ICE seems more irregular, it is still not exhibiting the same amount of ruggedness as the experiments. Both codes are underpredicting the icing limits. Neither of the codes shows the large horn structure on the lower side of the experimental ice shapes between $x=4\text{--}16\text{mm}$, despite accounting for gravity.

Ice Shape Variability

Ice accretion on airfoils is an inherently stochastic process. Previous studies indicate that ice shapes in icing wind tunnels can vary

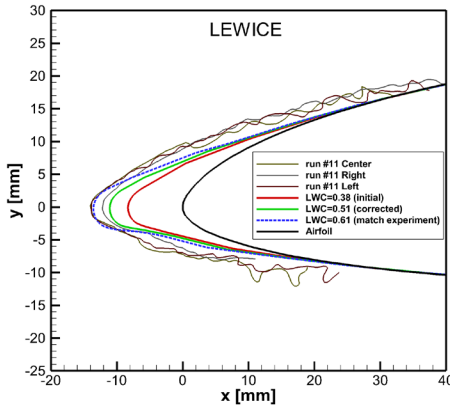


Figure 5. Comparison of experimental ice shapes to the numerical simulation results from LEWICE for the rime ice case.

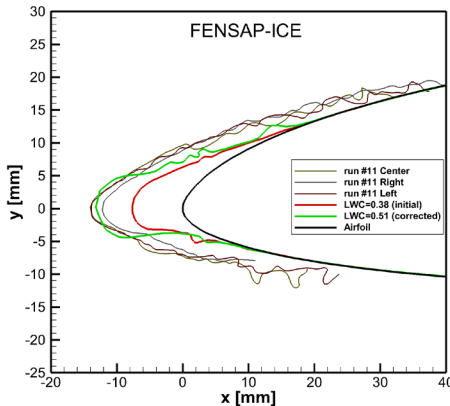


Figure 6. Comparison of experimental ice shapes to the numerical simulation results from FENSAP-ICE for the rime ice case.

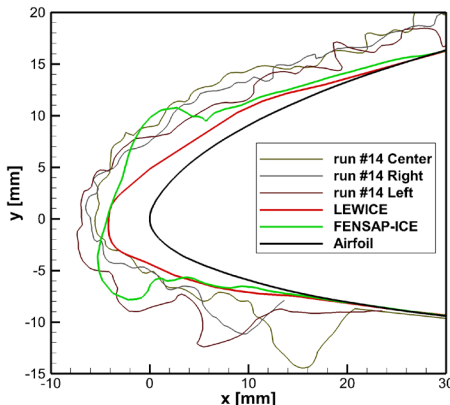


Figure 7. Comparison of experimental ice shapes to the numerical simulation results from LEWICE and FENSAP-ICE for the glaze ice case.

significantly between facilities, but also between runs [13]. As such it is of interest to investigate the variability and repeatability of the ice shape tracings. In this study, the temporal variability (between runs) and the spatial variability (along the span of the test section) was investigated.

Table 2 shows an overview of all experimental runs that have been considered to study the ice shape variability. The table shows the measured ice thicknesses as well as calculated results for thickness, area, and icing limits. For each set of identical runs, the mean \bar{x} is given along with the standard deviation σ .

Page 4 of 8

The comparison between the measured and calculated maximum thickness reveals that the post-processing of the ice tracings is not without fault. Differences ranging from $-1.6\ldots+2.5\text{mm}$ occur between the two methods. The reason why the calculated values diverge from the caliper measurements can be attributed to the manual tracing errors and the digitalization process. One challenge we found was to correctly capture the exact location of the airfoil in relation to the ice shape on the tracing papers.

Generally, the data shows the largest variations for the S826 airfoil, for the cases with an icing duration of 40min. The resulting ice shapes are very large and exhibit significantly higher variability in all characteristic parameters. The choice for the initial icing times of 40min was based on numeric simulations that were carried out before the experiments. When the large deviations between simulation and experiment – related to the LWC calibration issue – were detected, the icing times were consequently reduced to 20min for all tests on the RG-15 airfoil.

Figures 8–10 show the spanwise distribution of the ice area on the RG-15 airfoil for a rime, mixed, and glaze case with three identical runs each. The ice area is a good overall indicator of the accretion process. The results display that there is a considerable degree of temporal and spatial variability for all three cases. No consistent trends of more/less ice accretion on any side of the test section could be observed. However, it seems that the icing conditions have an impact on the degree of variability. The rime case exhibits a significantly lower amount of variation, compared to mixed and glaze, the latter showing the largest spread.

Icing limits have been identified on the upper and lower side of the airfoil. The variation of the limits appears to be consistent, with values varying within the range of 1–2cm. The only exception is the glaze case for the 40min test run, where the variation of the upper and the lower limit are significantly elevated. The RG-15 airfoil shows a clear trend for more ice accretion on the lower side, whereas the S826 exhibits a more symmetric ice distribution between the lower and upper side.

Ice Shape Acquisition

The main results in this study are based on manual tracings of ice shapes. The data suggests that there is a significant amount of variation of the ice shapes in the spanwise direction. This information is only partially captured, as only three locations were used for ice tracings. Furthermore, the manual tracing method is subjective and susceptible to variations, depending on the skill and experience of the person taking the measurements. This is the motivation to investigate other – more objective – methods to obtain ice shapes. Two methods have been tested. First, we used the Structure Sensor [23], which is a handheld 3D scanning device. The sensor is an accessory for iPads and captures its surroundings by infrared structured light technology. The scanner was used on the iced airfoil inside the wind tunnel. Figures 11–13 show different examples of the resulting ice geometries. In general, the ice shapes have been captured better than expected. It was anticipated that the ice shapes would be problematic to scan due to their optical properties (translucency & reflectivity). This, however, turned out not to be a major issue, which is likely related to the infrared technology of the scanner. However, we found that the resolution of the ice shapes was inconsistent. The scanned mesh consists of cells with lengths between 3–9mm length, which is relatively coarse. The resulting ice shapes are missing key features, such as feathers, clear icing limits and surface roughness. However, the 3D scans allow for a good assessment of the spanwise distribution

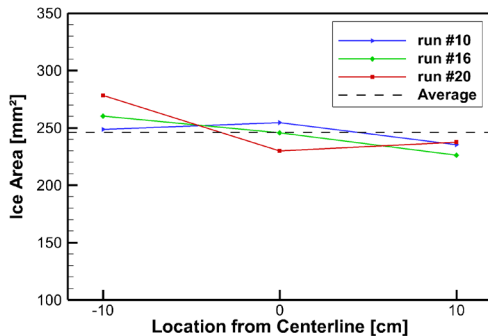


Figure 8. Calculated ice area for three identical rime ice runs.

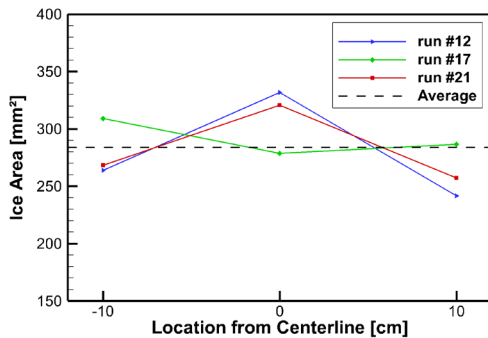


Figure 9. Calculated ice area for three identical mixed ice runs.

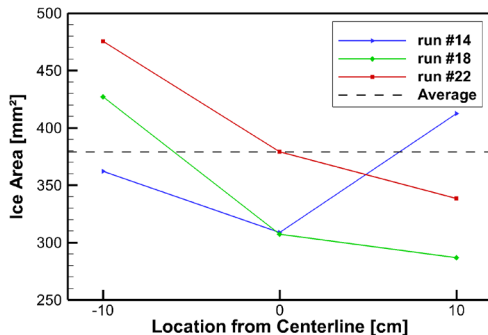


Figure 10. Calculated ice area for three identical glaze ice runs.

of ice, as best seen in Fig. 11. The shown case is a scan from a rime ice run (run #2) on the S826 airfoil. The scan was performed after the manual tracings have been taken, which can be seen from the three cuts in the ice. From the scan, it is obvious that less ice has accumulated on the left side. Ice thickness measurements based on the scanned data are matching well with the caliper measurements. Figure 12 shows a mixed ice case (run #8). The results clearly show the horn formation and how the horn is only occurring in the middle and right section of the model. A feature which is consistent with all scanned results is that the upper surface is much better resolved than the lower. This may be related to the handling of the device because it was easier for the person sitting inside the tunnel to scan the upper surface. For runs with less ice accretion, for example on the RG-15 airfoil in Fig. 13 (run #16), the ice shapes became less clear and less distinct.

The second method to acquire ice shapes was to use photogrammetry. This method allows creating 3D models based on multiple images of an object, taken from various locations and angles. For the model generation, the software Agisoft Photoscan [24] was used. First tests revealed that the optical properties of ice made it difficult to generate

an accurate model. For this reason, the ice was painted black with a fine brush, which significantly improved the results. Two approaches have been selected. First, ice segments have been carefully removed from the airfoil and placed in a freezer until further processing. The segments were then painted and returned to the freezer until the paint was dried. Then, the ice segments were placed in front of a white background and a series of pictures were taken from all direction. An example of the results is shown in Fig. 14 for a mixed ice shape. The resulting 3D model shows a good resolution of the ice geometry and are able to capture details well. Removal of intact ice shapes has been successful for most glaze and mixed cases, whereas the adhesion forces for rime ice was so high that it was often not possible to remove a segment without damaging it.

For this reason, the second approach was to take images of the ice while still attached to the airfoil, inside the wind tunnel. Figure 15 shows an unpainted rime ice shape that has been captured with this method. It was found that the method works reasonably well, although the surfaces features are less detailed compared to the previous photogrammetry result. The reason for this was the optical properties of ice. Painting the ice segment inside the tunnel proved to be difficult and time-consuming. Especially the drying process took very long, and the test was aborted. Pictures taken of a painted wet ice shape were not processable with the photogrammetry software due to excessive reflections of the surface.

Discussion

Obtaining high-fidelity ice shapes, that are representable for certain icing conditions and are suitable for the validation of numerical icing models comes with many intricate challenges. On the experimental side, there are several factors that can have a large impact on the resulting ice geometries. As shown in this study, the calibration of the LWC is a key issue, that may introduce a significant (systematic) error. The LWC problem in this campaign arose partly because of the lack of experience of testing at low Reynolds numbers and because testing was conducted at the lower limits of the wind tunnel capabilities. The effect of the blade collection coefficient and the off-specification icing blade were magnified by low tunnel speeds. The effects would have had significantly smaller at wind speeds which are typical for aviation, due to higher droplet inertia. It is important to highlight, that the LWC calibration problem was detected early in the testing phase due to the availability of simulation data. This underlines the benefits of conducting experimental work in close collaboration with numerical methods.

There are several other parameters that add to the uncertainty of the ice shape data. The MVD distribution has not been verified in the scope of this work and remains a significant unknown. The droplet sizes play an important role for the droplet impingement limits on the airfoil and may be responsible for the large observed deviations between the numerical and experimental data. This is an issue that must be investigated in further detail. Furthermore, the density of the ice is a variable that has not been tested and may affect ice shapes (and LWC calibration) to a large degree. It is highly recommended that future experiments focus on these uncertainties in order to build more confidence in the experimental data.

Investigations of the repeatability of the tests show a dependency on the icing type. For rime and mixed ice, the results exhibit a significantly lower variability compared to glaze. Since the numerical simulation of glaze ice is more challenging than for rime (due to the complex icing processes on the surface), the validation data for these cases are particularly interesting and require good confidence. The

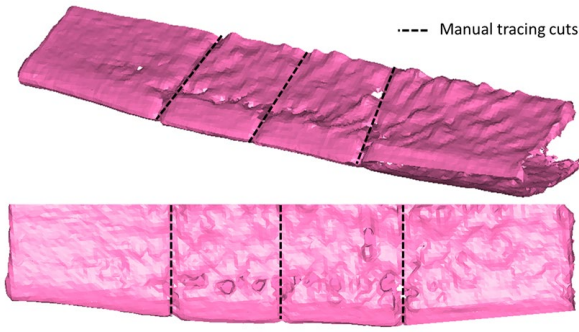


Figure 11. 3D scan results on a rime ice case with 40min duration.

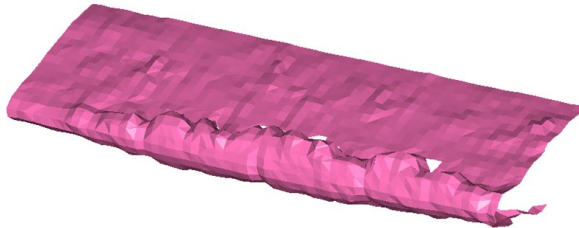


Figure 12. 3D scan results on a mixed ice case with 20min duration.

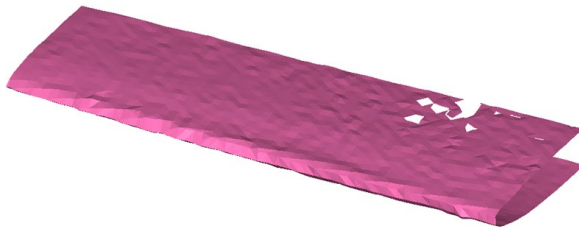


Figure 13. 3D scan results on a rime ice case with 20min duration.

preliminary numerical results show large deviations compared to the experimental glaze geometries, which indicates that special attention must be given to the accuracy of the experimental glaze data. One aspect is that spanwise distribution of ice is showing the largest variability for glaze. Therefore, it seems a good practice to take several spanwise ice tracings, which should not take too much additional time.

Last but not least, manual tracing of the ice comes with an inherent stochastic error that is related to the skill and experience of the experimenter. The post-processing of the tracings, especially the digitalization, also introduces errors. Using caliper measurements and comparing them to the calculated thicknesses has proven as a good method to identify large deviations and flag cases for re-processing to increase accuracy. In general, the manual process is very time-consuming and requires special attention to detail. For this reason, the exploration of alternative methods of ice shape capturing seems beneficial.

The 3D handheld scanner was able to capture the ice shapes well, however with a very low degree of detail. Further investigations are required on how to improve accuracy and how to reduce the large spread in the resolution. Otherwise, the method is very fast and may be very well suited for measuring spanwise distribution of ice, ice area, and icing limits. The second approach was to use photogrammetry on ice. This approach has shown to be very sensitive to the optical properties of ice. Clean ice, as well as painted ice that was still wet, was very difficult to process and yielded low-quality results. However, the specimen that have been painted and dried, have shown a very high level of detail and are well suited for further investigations. Such high-fidelity ice shapes are required for aerodynamic performance degradation studies, e.g. with CFD or experimental methods with 3D painted artificial ice shapes. One problem that is related to painting the ice is, that the painting procedure might alter the ice shape. An improvement that should be considered for both approaches is to add optical markers with known distances between each other. This information will help to set the correct scaling and to get the overall dimensions in the correct magnitude.

The icing simulation results can be considered as preliminary results for the validation of LEWICE and FENSAP-ICE for UAV applications. The rime case shows a good match with the experimental data in terms of general thickness and shape. However, icing limits and the ruggedness of the surface are not well represented. For glaze, the consistency with the experimental data is significantly worse. This may be related to the more complex icing processes inherent to the glaze ice formation, due to the presence of a freezing water film on the surface. At this stage, more detailed investigations are required to improve the predictive qualities of the numerical codes. There is a multitude of parameters that can be adjusted in order to obtain better predictions, in particular within FENSAP-ICE. Future work will focus on a more in-depth comparison of FENSAP-ICE and LEWICE to these experimental data.

Conclusion

The main goal of this study was to generate reliable experimental ice shape data for UAV icing applications at low Reynold numbers. Such data is required for the validation of numerical icing methods, which have typically been developed and verified for general aviation purposes. This study generated a large dataset containing the three main characteristic icing types: rime, mixed, and glaze. Special focus has been paid to investigate the variability of ice shapes. Cases have been run several times at identical icing conditions and manual ice tracings were taken at three spanwise locations. The results show that the degree of variability is depending on the ice type and is highest for glaze and lowest for rime. However, even for the glaze case, the variability is within moderate limits, and may therefore still be used for validation purposes.

Several sources of errors have been identified and addressed. A significant systematic error had been discovered, that was related to the calibration of the LWC. The icing wind tunnel facility is following the ARP5905 icing blade method, however with a blade that had different dimensions than required by the document. It was shown, that the thicker blade has a detrimental effect on the droplet collection coefficient at low flow velocities. Furthermore, the icing density used for the calibration has not been verified for these tests and was assumed with a potentially low value. These systematic errors have been accounted for and indicate that the actual LWC during the tests was much higher than initially planned.

A secondary goal of this study was to investigate novel methods to capture ice shapes. Two methods have been tested. A low-cost 3D scanner has been able to capture the overall ice shape on the airfoils using infrared technology. The resolutions of the resulting meshes were varying and generally found to be too coarse to capture fine details. However, bulk measurements such as spanwise distribution, ice area, and icing limits could potentially be performed with the device. The second approach was performed with image photogrammetry on ice segments. The optical properties of ice made it difficult to generate 3D point clouds. By painting the ice shapes, the outcome could be significantly improved, and very detailed ice shapes have been generated. This required the paint to dry first.

Icing simulations with FENSAP-ICE and LEWICE have been performed and compared to experimental rime and glaze shapes. These preliminary validation results show good general agreement with rime ice shapes. The ice geometry was well captured, however, differences in surface ruggedness and a lack of details were observed. For glaze ice, the agreement was significantly worse for both numerical codes. More work is planned to investigate the best parameter setting within the icing codes that will give the best predictions for UAV icing conditions. Further research questions are also related to the aerodynamic performance effects (lift, drag, stall) that are induced by these ice geometries.

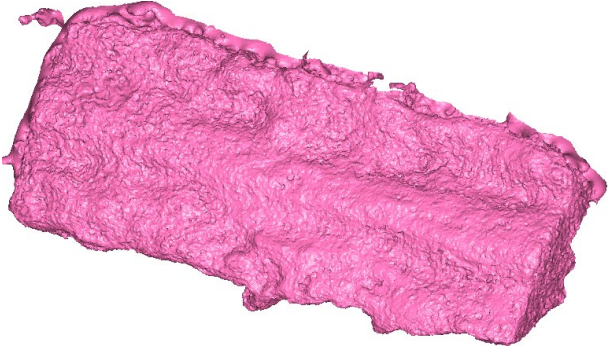


Figure 14. Photogrammetry result on a painted (dry) mixed ice segment that has been carefully removed from the airfoil.

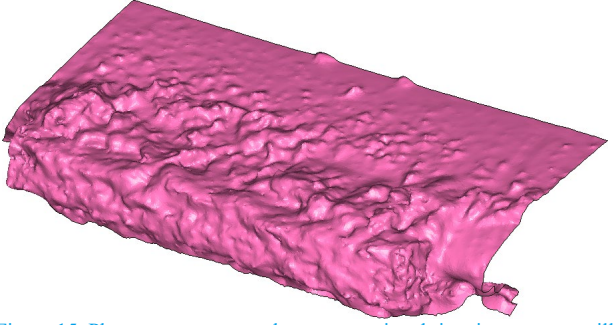


Figure 15. Photogrammetry result on an unpainted rime ice segment still attached to the airfoil

Table 2. Overview of ice accretion runs with measured ice thicknesses, as well as calculated ice thickness, area, and limits.

Run ID	Airfoil	Config	Time	Max. thick. measured			Max. thick. calculated			Ice area			Lower ice limit			Upper ice limit		
				[min]	[mm]		[mm]			[mm ²]			[s/c]			[s/c]		
run #1	S826	Rime 1	40	23.5	17.6	28.3	25.0	18.4	26.8	450	515	599	-0.11	-0.12	-0.08	0.13	0.11	0.17
run #2	S826	Rime 1	40	25.7	27.0	23.5	24.1	27.1	22.8	451	543	458	-0.10	-0.11	-0.10	0.17	0.18	0.19
				$\bar{x} = 24.3 \sigma = \pm 3.8$			$\bar{x} = 24.1 \sigma = \pm 3.2$			$\bar{x} = 503 \sigma = \pm 61$			$\bar{x} = -0.10 \sigma = \pm 0.01$			$\bar{x} = 0.16 \sigma = \pm 0.03$		
run #4	S826	Glaze 1	40	12.6	11.7	13.5	11.8	12.8	12.5	699	740	879	-0.11	-0.13	-0.14	0.05	0.17	0.18
run #5	S826	Glaze 1	40	12.8	10.3	13.0	11.8	11.7	13.1	853	543	718	-0.20	-0.20	-0.10	0.05	0.19	0.05
				$\bar{x} = 12.3 \sigma = \pm 1.2$			$\bar{x} = 12.3 \sigma = \pm 0.6$			$\bar{x} = 739 \sigma = \pm 121$			$\bar{x} = -0.15 \sigma = \pm 0.04$			$\bar{x} = 0.12 \sigma = \pm 0.07$		
run #10	RG-15	Rime 1	20	15.1	14.4	14.4	13.9	12.8	13.3	230	246	255	-0.10	-0.13	-0.13	0.03	0.05	0.06
run #16	RG-15	Rime 1	20	14.5	13.1	13.8	12.5	12.0	13.3	238	226	235	-0.13	-0.12	-0.11	0.03	0.05	0.04
run #20	RG-15	Rime 1	20	16.2	14.5	15.0	14.4	12.7	13.3	278	260	249	-0.14	-0.14	-0.12	0.05	0.04	0.04
				$\bar{x} = 14.6 \sigma = \pm 0.9$			$\bar{x} = 13.1 \sigma = \pm 0.7$			$\bar{x} = 246 \sigma = \pm 16$			$\bar{x} = -0.12 \sigma = \pm 0.01$			$\bar{x} = 0.04 \sigma = \pm 0.01$		
run #12	RG-15	Mixed 1	20	14.7	13.1	14.0	13.2	11.7	13.2	321	279	332	-0.12	-0.14	-0.11	0.04	0.06	0.07
run #17	RG-15	Mixed 1	20	13.5	13.5	14.4	11.1	11.2	12.8	257	287	242	-0.11	-0.15	-0.11	0.05	0.05	0.03
run #21	RG-15	Mixed 1	20	14.4	12.8	13.4	13.7	13.5	13.7	268	309	264	-0.12	-0.15	-0.11	0.05	0.04	0.05
				$\bar{x} = 13.8 \sigma = \pm 0.7$			$\bar{x} = 12.7 \sigma = \pm 1$			$\bar{x} = 284 \sigma = \pm 30$			$\bar{x} = -0.12 \sigma = \pm 0.02$			$\bar{x} = 0.05 \sigma = \pm 0.01$		
run #14	RG-15	Glaze 1	20	6.5	6.0	6.2	5.8	6.5	7.8	379	307	309	-0.16	-0.18	-0.17	0.09	0.04	0.06
run #18	RG-15	Glaze 1	20	7.1	6.3	6.9	7.0	7.5	7.8	338	287	413	-0.16	-0.19	-0.16	0.06	0.06	0.09
run #22	RG-15	Glaze 1	20	7.0	6.2	6.8	7.3	6.2	5.3	476	427	362	-0.18	-0.19	-0.16	0.08	0.05	0.06
				$\bar{x} = 6.6 \sigma = \pm 0.4$			$\bar{x} = 6.8 \sigma = \pm 0.9$			$\bar{x} = 366 \sigma = \pm 63$			$\bar{x} = -0.17 \sigma = \pm 0.01$			$\bar{x} = 0.07 \sigma = \pm 0.02$		

References

1. Siquig, A., "Impact of Icing on Unmanned Aerial Vehicle (UAV) Operations," Naval Environmental Prediction Research Facility, 1990.
2. Hann, R., "Opportunities and Challenges for Unmanned Aerial Vehicles (UAVs) in the Arctic," *13th ArcticNet Annual Scientific Meeting*, 2017.
3. Peck, L., Ryerson, C.C., and Martel, C.J., "Army Aircraft Icing Cold Regions Research and Engineering Laboratory," (September), 2002.
4. Bragg, M.B., Broeren, A.P., and Blumenthal, L.A., "Iced-airfoil aerodynamics," *Prog. Aerosp. Sci.* 41(5):323–362, 2005, doi:10.1016/j.paerosci.2005.07.001.
5. Szilder, K. and McIlwain, S., "In-Flight Icing of UAVs -

- The Influence of Reynolds Number on the Ice Accretion Process,” SAE Technical Paper 2011-01-2572, 2011, doi:10.4271/2011-01-2572.
6. Koenig, G.G., Ryerson, C.C., and Kmiec, R., “UAV Icing Flight Simulation,” *40th Aerospace Sciences Meeting & Exhibit*, AIAA-2002-0812, Reno, 2002.
 7. Tran, P., Baruzzi, G., Tremblay, F., Benquet, P., Habashi, W.G., Petersen, P.B., Liggett, M.W., and Fiorucci, S., “FENSAP-ICE applications to unmanned aerial vehicles (UAV),” *42nd AIAA Aerospace Sciences Meeting and Exhibit*, 390–402, 2004.
 8. Szilder, K. and Yuan, W., “In-flight icing on unmanned aerial vehicle and its aerodynamic penalties,” *Prog. Flight Phys.* 9:173–188, 2017, doi:10.1051/eucass/201709173.
 9. Hann, R., “UAV Icing: Comparison of LEWICE and FENSAP-ICE for Ice Accretion and Performance Degradation,” *2018 Atmospheric and Space Environments Conference*, AIAA Aviation, Atlanta, ISBN 978-1-62410-558-6, 2018, doi:10.2514/6.2018-2861.
 10. Hann, R., “UAV Icing: Comparison of LEWICE and FENSAP-ICE for Anti-Icing Loads,” *AIAA Scitech 2019 Forum*, AIAA, San Diego, ISBN AIAA 2019-1286, 2019, doi:10.2514/6.2019-1286.
 11. Williams, N., Benmeddour, A., Brian, G., and Ol, M., “The effect of icing on small unmanned aircraft low Reynolds number airfoils,” *17th Australian International Aerospace Congress*, AIAC, Melbourne, 2017.
 12. Liu, Y., Li, L., and Hu, H., “Effects of Ice Accretion on the Aerodynamic Performance and Wake Characteristics of an UAS Propeller Model,” *2018 Atmos. Sp. Environ. Conf.* 1–17, 2018, doi:10.2514/6.2018-3496.
 13. Aerospace Information Report, “Icing Wind Tunnel Interfacility Comparison Tests,” AIR5666, 2012.
 14. Battisti, L., “Wind Turbines in Cold Climates,” Springer, 2015.
 15. Hammond, D.W. and Luxford, G., “The Cranfield University Icing Tunnel,” *41st Aerospace Sciences Meeting and Exhibit*, 2003.
 16. Rohatgi, A., “WebPlotDigitizer,” www.automeris.io/WebPlotDigitizer, Date: February, 2019.
 17. Habashi, W.G., Aubé, M., Baruzzi, G., Morency, F., Tran, P., and Narramore, J.C., “FENSAP-ICE : A Fully-3D in-Flight Icing Simulation System for Aircraft , Rotorcraft and UAVs,” *24th International Congress of the Aeronautical Sciences*, ICAS, 2004.
 18. SAE International, “ARP5905 Calibration and Acceptance of Icing Wind Tunnels,” Aerospace Recommended Practice ARP5905, 2015.
 19. Macklin, W.C., “The density and structure of ice formed by accretion,” *Q. J. R. Meteorol. Soc.*, 1962.
 20. Jones, K.F., “The density of natural ice accretions related to nondimensional icing parameters,” *Q. J. R. Meteorol. Soc.*, 1990.
 21. Vargas, M., Broughton, H., Levy, P., Sims, J.J., Bleeze, B., and Gaines, V., “Local and Total Density Measurements in Ice Shapes,” *J. Aircr.*, 2007.
 22. NATO RTO Technical Report 38, “Ice Accretion Simulation Evaluation Test,” RTO-TR-038 AC/323(AVT-006)TP/26, 2001.
 23. Occipital Inc, “Structure sensor,” www.structure.io/structure-sensor, Date: February 2019, Sep. 2003.
 24. AgiSoft, “PhotoScan Professional,” www.agisoft.com/downloads/installer, Date: February 2019.

Contact Information

Richard Hann, richard.hann@ntnu.no
O.S. Bragstads plass 2D, NO7491 Trondheim, Norway

Acknowledgments

This project has received funding from the Research Council of Norway under grant number 237906, Centre for Integrated Remote Sensing and Forecasting for Arctic Operations (CIRFA). The research was also funded by grant number 223254, Centre for autonomous marine operations and systems (NTNU AMOS). I would like to thank my colleagues from NTNU helping with testing, Kasper Trolle Borup and Artur Piotr Zolich. Special thanks goes to Hugo Pervier and Peter West from Cranfield University, who were an integral part of this work and were very helpful at all times.